A Platinum Open Access Journal for Organic Chemistry

Paper

Free to Authors and Readers | DOAJ Seal | *Arkivoc* **2025** (3) 202512521

Selective photocatalytic synthesis of quinoxaline derivatives by Cu/Pd-N-TiO_2 as an efficient heterogeneous photocatalyst

Berlinda M. Sikakane,[a] Ross S. Robinson,*[a] Timothy M. Underwood[b] and Matthew Akerman[a]

[a]School of Agriculture & Science, University of KwaZulu-Natal, Pietermaritzburg, South Africa
[b]Catalysis Institute, University of Cape Town, Cape Town, South Africa
Email: RobinsonR@ukzn.ac.za

Dedicated to Prof. H.-G. Schmalz

Received 12-09-2025 **Accepted** 06-04-2026 **Published on line** 06-14-2026

Abstract

A highly efficient and recyclable photocatalyst Cu/Pd-N-TiO_2 was developed and used successfully for a one-pot synthesis of twenty 2-substituted and 2,3-disubstituted quinoxaline derivatives by the reaction of various alpha-hydroxyketones with ortho-phenylenediamines. The composition and crystal phase of the catalyst were determined by p-XRD studies, and its morphological and surface characteristics were ascertained by SEM and HRTEM studies. All the synthesized compounds were appropriately identified by spectroscopic studies (IR, ^{1}H and ^{13}C NMR, MS)

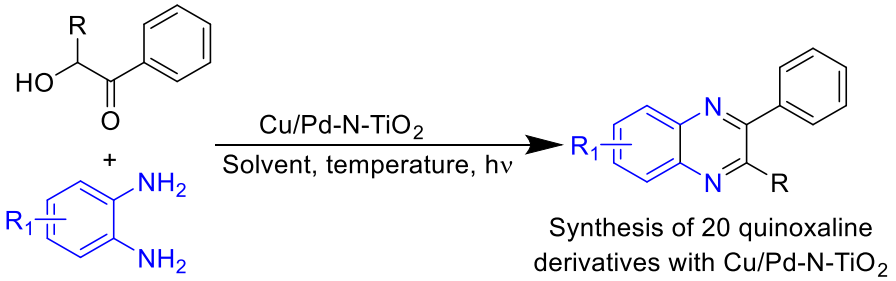

Synthesis of 20 quinoxaline derivatives with Cu/Pd-N-TiO_2 as a recyclable catalyst, 60-99% conversions

Keywords: Photo-catalysis; titanium dioxide; oxidation; quinoxaline; Wittig

Introduction

Heterogeneous catalysts are widely used in industrial chemical processes due to their ability to increase reaction rates and product yields, their ease of separation from the reaction mixture, and their potential recyclability.[1] Among the heterogeneous catalysts, titanium dioxide (TiO_2) is a widely studied and used metal oxide semiconductor. Its widespread application is the result of the photo-generated holes and electrons, which have attracted significant research within photocatalysis. However, TiO_2 possesses a major drawback of being unable to utilize the visible light region of the electromagnetic spectrum for photocatalytic processes. To overcome this, doping with metals and organic compounds such as carbon and nitrogen, and visible light-responsive metals, for example, Au and Pd has been described.[2] This can also reduce the potential for recombination of electron-hole pairs.[3]

In recent years, TiO_2 nanoparticles have been applied as heterogeneous photocatalysts in light-driven pollutant degradation studies,[4-7] however, this has attracted a growing interest towards light-driven catalytic organic synthesis.[8-10] The use of photocatalysis as an alternative to conventional synthetic pathways has proven to be a cost-effective and eco-friendly alternative. Heidari and co-workers prepared chlorophyll b-modified TiO_2 for the synthesis of tetrahydroquinoline derivatives under visible light. They obtained them in good yields, and the system was reusable six times with only a 13% decrease in activity.[11] It is of significance to seek and develop new strategies for selective and stable photocatalysts. This could be addressed by exploring and developing advanced methodologies capable of tailoring the electronic and chemical structures of photocatalysts. Recently, TiO_2 and metal-loaded/TiO_2 photocatalysts have been reported to carry out organic coupling reactions such as C-C bond formation and C-N bond formation for the synthesis of bioactive compounds.[12] Wu and co-workers developed a method utilizing light and recyclable TiO_2 photocatalysts for phenol and alkenylphenol oxidative coupling reactions.[13]

Among the various classes of heterocyclic compounds, such as quinolines, imidazoles and thiazoles, the quinoxalines form an important component of pharmacologically active compounds.[14-16] They are associated with a range of biological activities such as anticancer,[17] antifungal,[18] antimicrobial[19] among others.[20-22] They are obtained through diverse methods of synthesis and a range of starting materials, but the most common one is the condensation of 1,2-diketones and 1,2-diamines.[23]

Taylor *et al.*[24] developed a unique approach of performing a quinoxaline synthesis, whereby the reactants were introduced all together, in one go, known as the "tandem oxidation procedure" of α-hydroxy ketones into quinoxalines via in-situ trapping with aromatic 1,2-diamines, and found that the palladium system carried out the transformations efficiently. Cho *et al.*[25] used $CuCl_2$/molecular sieve 4Å system for the synthesis of quinoxalines in high yields from α-hydroxyketones and *o*-phenylenediamines.

From previous work published within this group Cu/Pd-N-TiO_2 was employed to mediate aerobic alcohol oxidation reactions to carbonyl compounds, achieving near-quantitative conversions and high selectivity.[26] In this present research, the scope was extended by applying the Cu/Pd-N-TiO_2 catalyst in tandem oxidation reactions for the synthesis of quinoxaline derivatives. The α-hydroxy ketones underwent oxidation to 1,2-diketones and then coupled with aromatic 1,2 diamines to produce quinoxalines through a one-pot synthesis utilizing air as a clean source.

Results and Discussion

Characterization of the catalyst Cu/Pd-N-TiO_2

The composition and crystal phase of Cu/Pd-N-TiO_2 was analyzed through powder X-ray Diffraction measurement (p-XRD). The p-XRD spectrum is reported in Figure 1. The diffraction peaks are consistent with

the anatase phase of TiO_2 (PDF card-211272),[27] which appeared at 25.26°, 37.89°, 47.93°, 54.42°, 62.66°, 68.77°, 70.14°, 75.06°, 80.75°, and 82.68°, and whose corresponding crystal planes are (101), (004), (200), (105), (204), (116), (220), (215), (008) and (224). There are no diffraction peaks representing Cu/CuO and Pd/PdO presence in the diffractogram because the amount of copper and palladium used was below the detection limit of p-XRD. These results are consistent with previously reported results in literature.[28] This also suggests that the incorporated N, Pd, and Cu into the lattice did not change the dimensions of the unit cell or the crystallinity.[29] No diffraction peaks indicate the presence of a rutile phase. The crystallite size of 7.74 nm was calculated using the Scherrer equation (Equation 1).

$$D_P = \frac{k\lambda}{\beta \cos \theta} \quad \textbf{(1)}$$

Where Dp = crystallite size, k = constant 0.89, λ = X-ray wavelength (nm), θ = angle of diffraction, and β = half width of the different peak (FWHM) of the 101 reflections of anatase.

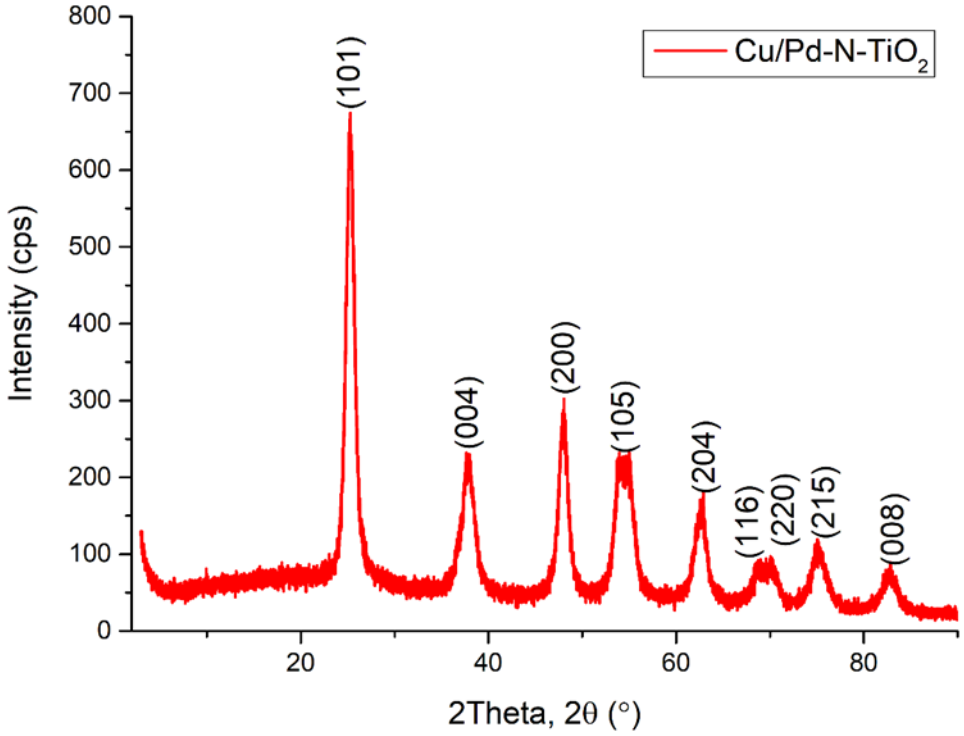

Figure 1. Powder-XRD of Cu/Pd-N-TiO_2 nanoparticles indexed to the PDF card-211272 of anatase, no Cu or Pd peaks evident.

The morphological and surface characteristics of the synthesized Cu/Pd-N-TiO_2 catalyst were studied using scanning electron microscopy (SEM) and high-resolution transmission electron microscopy (HRTEM). The SEM micrograph of Cu/Pd-N-TiO_2 nanoparticles has been noted in Figure 2(a), where aggregated irregular-shaped flakes can be observed. The transmission electron microscopy (TEM) micrograph of the nanoparticles in Figure 2(b) shows that the large cubic particles are agglomerated as observed by the red-circled region, and the smaller sphere-like particles are evenly distributed as observed by the green-circled region. HRTEM was

used to find the lattice fringes (Figure 2(c)), and the interplanar spacings of 0.355 nm, 0.358 nm, and 0.361 nm for (101) facet of anatase TiO_2 were observed, which is consistent with p-XRD results. The energy-dispersive X-ray spectroscopy (EDS) was used to confirm the elemental composition of the prepared catalyst, and the peaks for titanium, oxygen, nitrogen, copper, and palladium were observed (Figure 3). Copper and palladium had the lowest weight percentages compared with titanium, which further supports why their diffraction peaks were not observed on the p-XRD diffractogram. The EDS analysis was re-run without the contribution of titanium on the weight percentage due to an overlap with the nitrogen peak, which can be observed in figure 3(b).

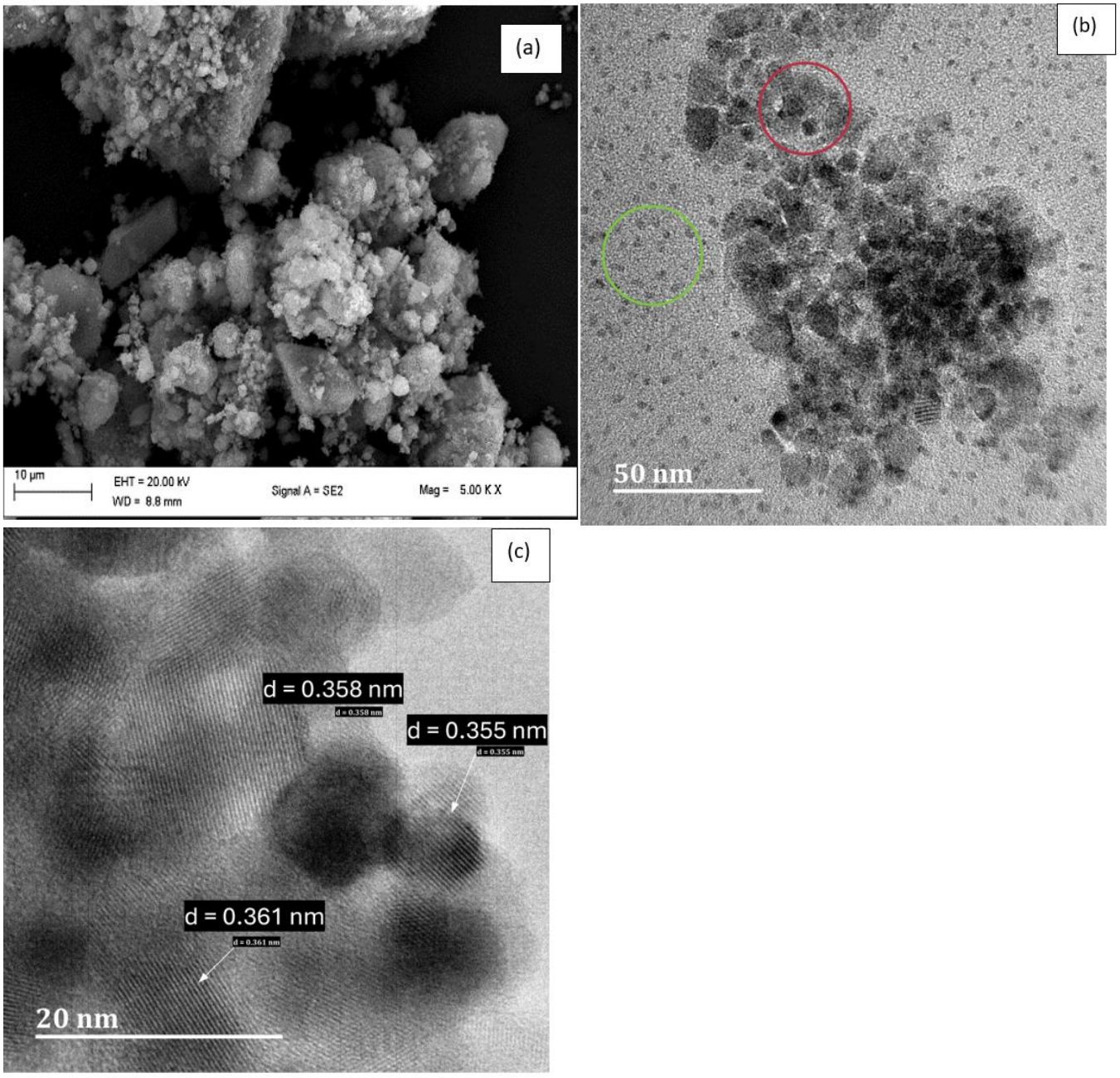

Figure 2. (a) Scanning electron micrograph of Cu/Pd-N-TiO_2. (b) Transmission electron micrograph of Cu/Pd-N-TiO_2. (c) HRTEM micrograph of Cu/Pd-N-TiO_2.

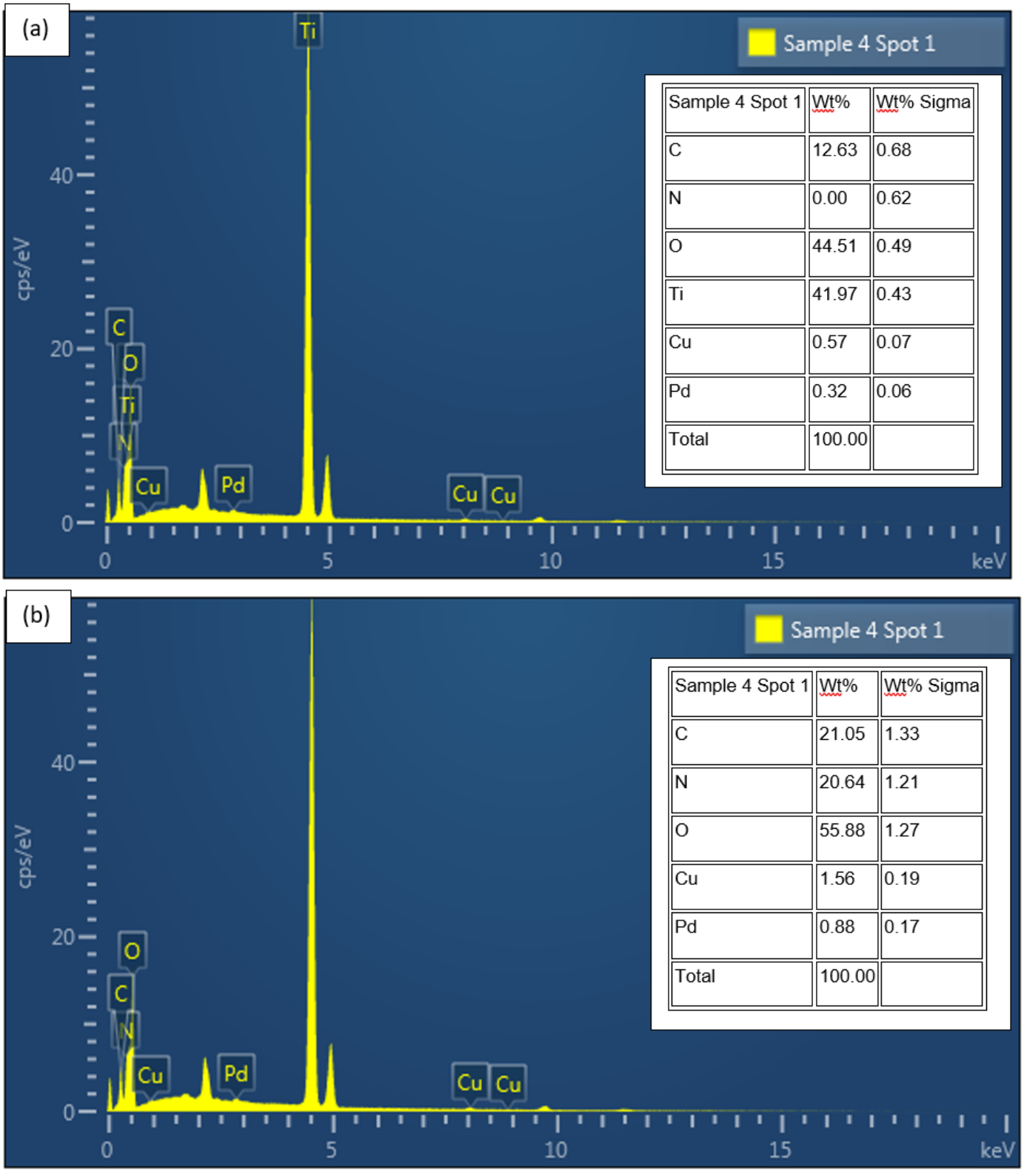

Figure 3. (a) Energy-dispersive X-ray spectroscopy analysis of Cu/Pd-N-TiO_2; insert: weight percentage contribution including titanium Kα, (b) Energy-dispersive X-ray spectroscopy analysis of Cu/Pd-N-TiO_2 insert: weight percentage contribution excluding the titanium Kα.

The N_2 physisorption experiment of Cu/Pd-N-TiO_2 is displayed in Figure 4. The surface area was found to be 119.851 m^2/g, and the average pore size was 4.866 nm, which is within the range of 2-50 nm of mesoporous materials, suggesting that the synthesized NPs are mesoporous materials. The large surface area of mesoporous compounds provides more active sites for adsorption and for organic reactions to take place. The catalyst's support plays an important role in the activity and selectivity of the catalyst. The isotherm corresponds well with type IV with hysteresis loops in the relative pressure range of 0.35-0.98. This type of adsorption isotherm suggests that the catalyst has a finite number of adsorbed molecules per site.[30] Zedan et al. in their study found that upon incorporation of Pd and Cu on TiO_2, there was a decrease in the surface area which led to an enhanced activity towards CO oxidation reaction.[28]

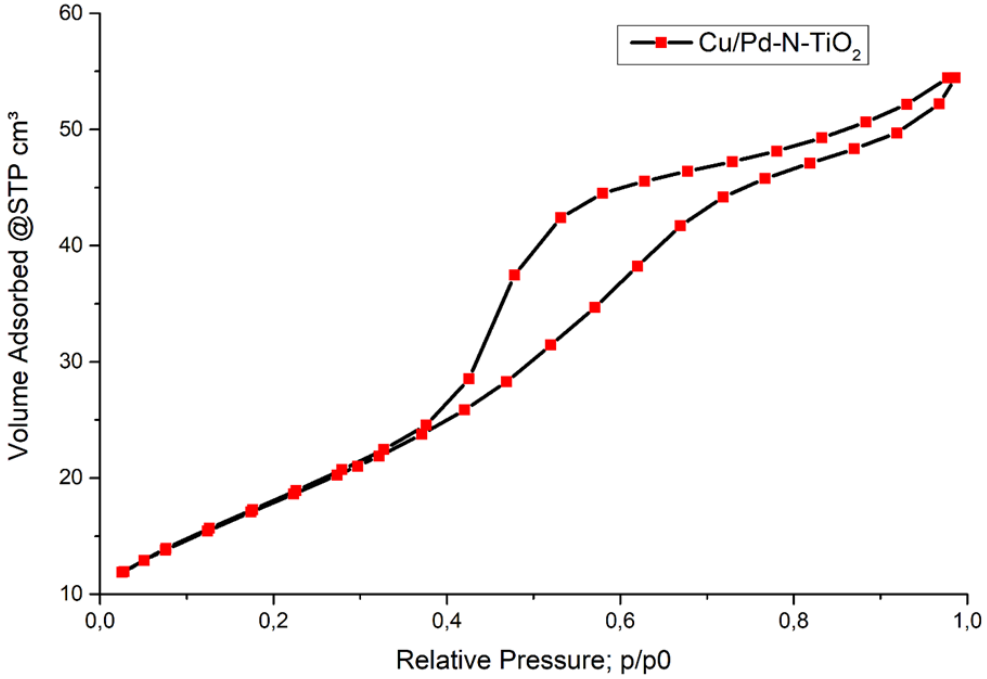

Figure 4. N_2 adsorption-desorption isotherm of Cu/Pd-N-TiO_2**.**

To evaluate the photocatalytic activity of the catalyst, the optical property of Cu/Pd N TiO_2 was investigated by UV-Vis diffuse reflectance spectra (UV-DRS). Figure 5 displays the UV-DRS spectrum and band gap energy calculated using Tauc's relation (Equation 2). The Tauc plot was used to estimate the band gap of titanium dioxide nanoseeds and Cu/Pd-N-TiO_2 nanoparticles.

$$(\alpha h\nu) = \mathrm{A}\left(h\nu - \mathrm{E}_g\right)^n \quad \textbf{(2)}$$

Where α, Eg, h, v, n, and A are absorption coefficients, band gap (eV), Planck's constant (6.6260 x 10^{-34} J.s), frequency of light, number characterizing transition (TiO_2 = ½) and a constant, respectively.

The optical absorption edge for TiO_2 nanoseeds and Cu/Pd-N-TiO_2 nanoparticles is located at 400 nm and 454 nm, respectively. The comparison of the two absorption edges reveals that Cu/Pd-N-TiO_2 is red-

shifted toward longer wavelengths compared with TiO_2 and the energy required for transition is reduced. This is due to the incorporated nitrogen, copper, and palladium which offers the reduction of the recombination rate between photoexcited electron and hole. Tauc's relation was used to calculate the energy band gap. A decrease in the band gap energy from 3.00 eV to 2.50 eV after modification with copper, palladium, and nitrogen, suggests that doping with copper, nitrogen, and palladium introduced new electronic levels, therefore, easier transitions from the valence band to the conduction band, resulting in higher photocatalytic efficiency.[31]These results are consistent with literature for Pd/Cu-TiO_2,[32] and N-TiO_2.[33]

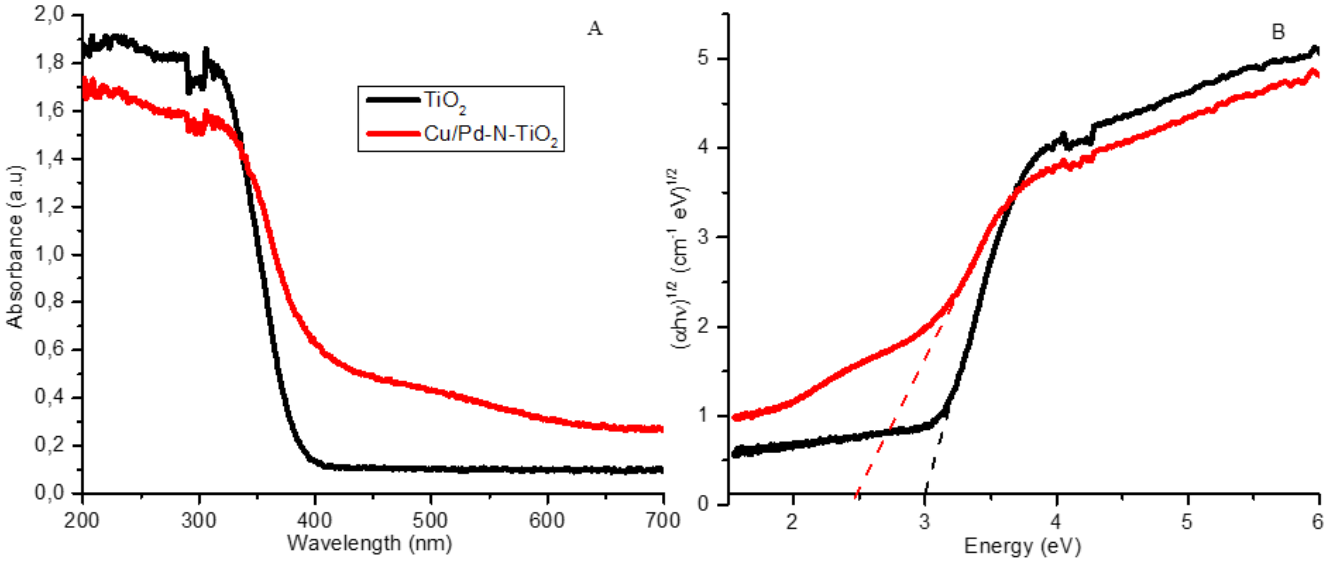

Figure 5. (a) UV-Vis diffuse reflectance spectra (UV-DRS), (b) Tauc plot of Cu/Pd-N-TiO_2. The spectra demonstrate the redshift after functionalization of TiO_2 with copper, palladium and nitrogen.

Synthesis of quinoxaline derivatives

The prepared Cu/Pd-N-TiO_2 was then used as the photocatalyst for the preparation of quinoxaline derivatives. The results of several oxidative cyclizations of 2-hydroxyacetophenone with o-phenylenediamine under various conditions are listed in Table 1. Tetrahydrofuran (THF) was the most suitable solvent at room temperature (**1-3**), with a 67% conversion within one hour. At 60 °C, the most suitable solvent for this reaction, with a conversion percentage of ≥ 99% under 6 h for 2-phenylquinoxaline (**6**) was THF. This may be attributed to the UV cutoff wavelength of THF (~212 nm) being lower than the lamp's emission wavelength, along with its high oxidation potential and polar aprotic nature.[34, 35] These properties, along with elevated temperatures, enhance catalyst activation and strengthen substrate interactions.

The reaction at room temperature for six hours without light irradiation (**7**) did not convert the starting material. This suggested that irradiation was necessary for the reaction to proceed and that Cu/Pd-N-TiO_2 functioned as a photocatalyst. The desired product was not detected in the absence of a catalyst (**8**), suggesting that the presence of the catalyst was essential for both the oxidation and cyclization steps of the reaction.

Table 1. Effect of solvents, temperature, and catalyst type for the synthesis of 2- phenylquinoxaline

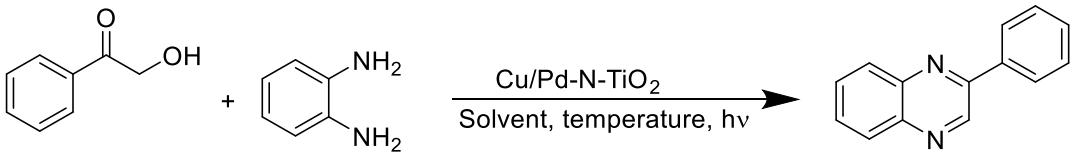

Entry	Catalyst	Solvent	Time (h)	Conv. (%)
1	Cu/Pd-N-TiO_2	Toluene (r.t)	1	11
2	Cu/Pd-N-TiO_2	Methanol (r.t)	1	13
3	Cu/Pd-N-TiO_2	Tetrahydrofuran (r.t)	1	67
4	Cu/Pd-N-TiO_2	Toluene (60°C)	1	26
5	Cu/Pd-N-TiO_2	Methanol (60°C)	1	27
6	Cu/Pd-N-TiO_2	**Tetrahydrofuran (60°C)**	**6**	**99**
7[A]	Cu/Pd-N-TiO_2	Tetrahydrofuran (rt)	6	0
8[B]	-	Tetrahydrofuran (60°C)	6	0
9	ZnO	Tetrahydrofuran (60°C)	1	46
10	MnO_2	Tetrahydrofuran (60°C)	1	35
11	TiO_2 nano seeds	Tetrahydrofuran (60°C)	1	50
12	Pd-N-TiO_2	Tetrahydrofuran (60°C)	1	78
13	Cu-N-TiO_2	Tetrahydrofuran (60°C)	1	59
14	Cu/Pd-N-TiO_2	Tetrahydrofuran (60°C)	1	99

Reaction conditions: (0.1 mmol) *o*-phenylenediamine, (0.1 mmol) 2-hydroxyacetophenone, catalyst in 3 mL solvent, [A]without light-irradiation, [B]without catalyst, *r.t.*; room temperature.

A comparative study of common metal oxides (ZnO, MnO_2) and different variations of the current catalyst (TiO_2 nanoseeds, Pd-N-TiO_2, and Cu-N-TiO_2) against the current catalyst Cu/Pd-N-TiO_2 was also done to demonstrate the effectiveness of this method (**11-13**). These reactions were done for 1 hour under irradiation and at 60 °C. Notably, Pd-N-TiO_2 achieved 78% yields which is high compared to the other systems, but the synergistic bimetallic Cu/Pd system on N-TiO_2 (**14**) gave the highest yield of 99% in one hour. This synergistic effect likely arises from enhanced electron transfer and active site availability due to the combined catalytic properties of Cu and Pd.[29, 36]

Therefore, based on the observations found (as reported in Table 1) the acquired optimal reaction conditions (THF, 6 h, 60 °C) were identified. Thereafter, the synthesis of a wide range of quinoxaline derivatives was performed, and the results are summarized in Table 2. All products were characterized by ^{1}H and ^{13}C NMR, FTIR, and TOF-MS and percentage conversions were determined from relative ^{1}H NMR integrals of reactant and product signals, assuming proportionality between signal area and concentration under quantitative conditions. Various electron-donating (e.g -Me, -OMe) and withdrawing groups (e.g. -CHO, -Br, -Cl,) substituted on hydroxy ketones and diamines were also evaluated. This was done to explore the efficiency of the methodology, and no significant influence of electron-rich and electron-deficient groups was observed since good yields with high purity were obtained. However, the catalyst displayed poor photocatalytic activity towards the cyclization of hydroxy acetone and diamines **(5a-d)**.

Table 2. Synthesis of various quinoxaline derivatives with Cu/Pd-N-TiO_2 as a catalyst

Entry	Hydroxy ketone	Diamine	Product	Conv. (%)
1a	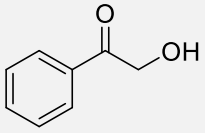	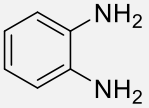	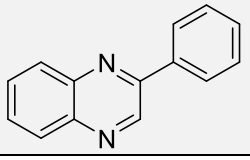	90
1b	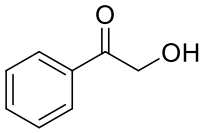	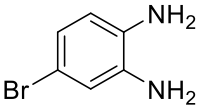	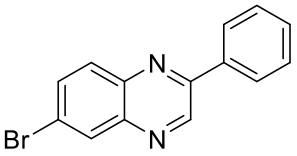 (+ regioisomer)	90
1c	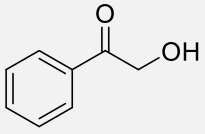	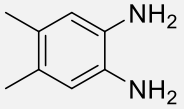	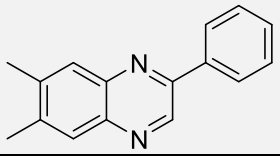	99
1d	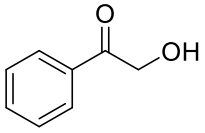	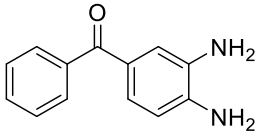	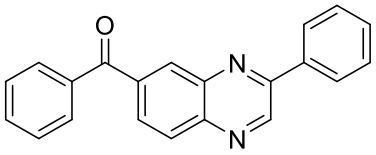 (+ regioisomer)	90
2a	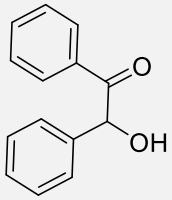	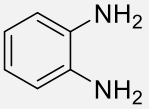	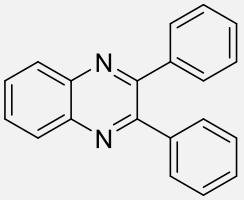	99
2b	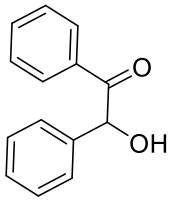	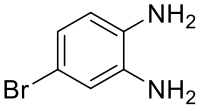	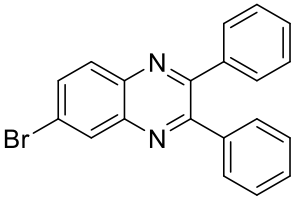	84

Table 2. Continue

Entry	Hydroxy ketone	Diamine	Product	Conv. (%)
2c	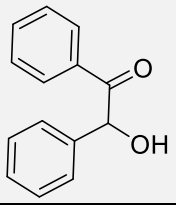	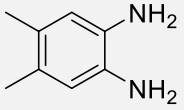	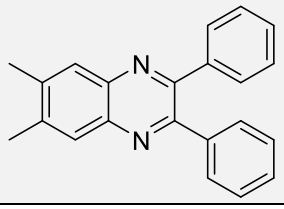	99
2d	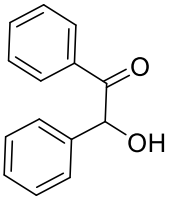	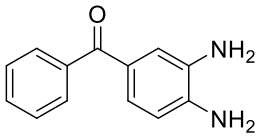	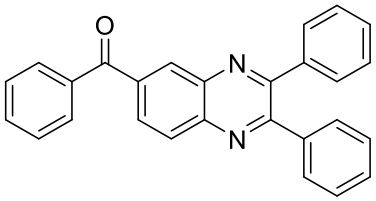	89
3a	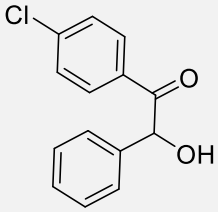	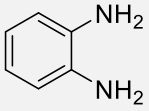	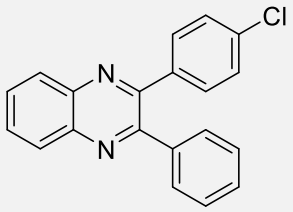	99
3b	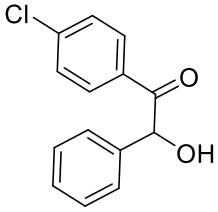	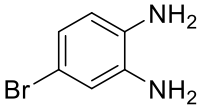	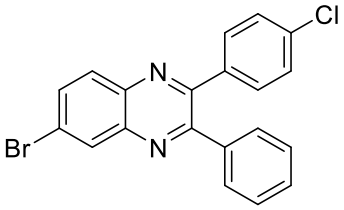 (+ regioisomer)	92
3c	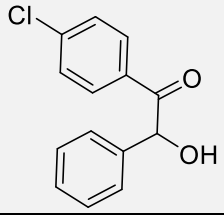	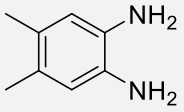	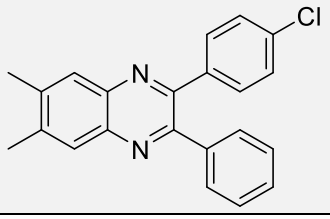	99
3d	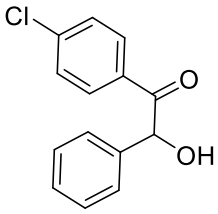	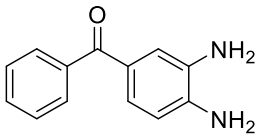	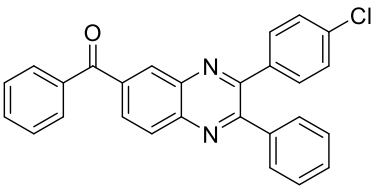 (+ regioisomer)	88
4a	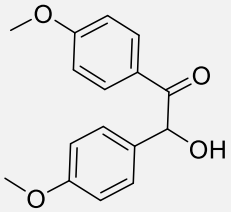	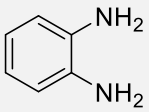	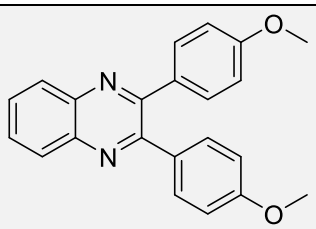	99

Table 2. Continue

Entry	Hydroxy ketone	Diamine	Product	Conv. (%)
4b	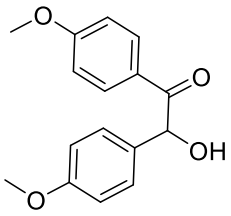	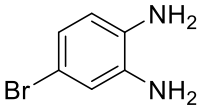	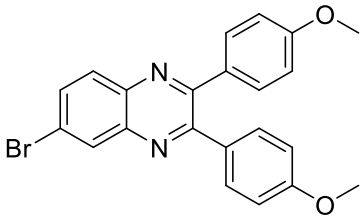	85
4c	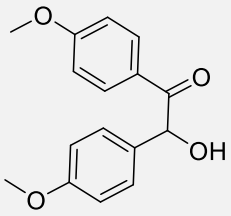	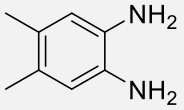	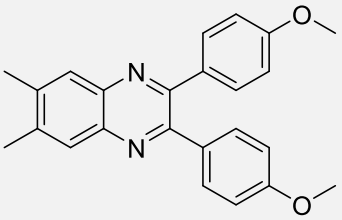	70
4d	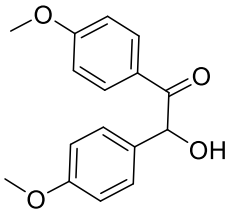	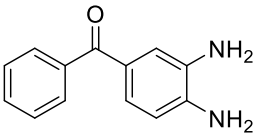	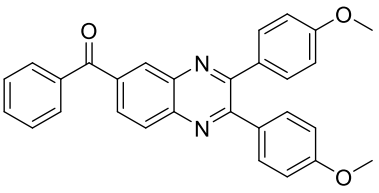	78
5a	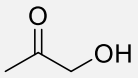	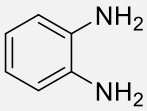	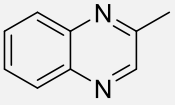	0
5b	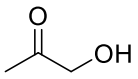	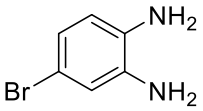	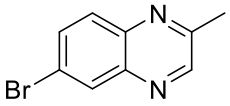 (+ regioisomer)	60
5c	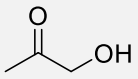	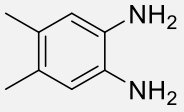	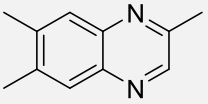	0
5d	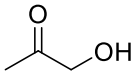	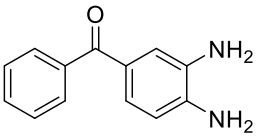	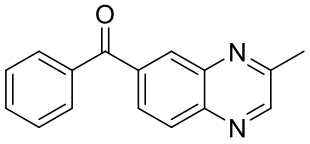 (+ regiosiomer)	0

The recyclability of Cu/Pd-N-TiO_2 was studied using the synthesis of 2-phenylquinoxaline (Figure 6). The catalyst showed excellent stability, maintaining 99% conversion through the third catalytic cycle, though the activity dropped to 53% in the fourth cycle, indicating a decline in catalytic activity. The decline in catalytic activity may be due to carbon deposition hindering the passage of organic substances through the pores to the active sites.[37, 38] This is further supported by the FTIR spectrum of the catalyst after four successive runs provided in Supplementary Material (Figure S40) which exhibits characteristic absorption bands at 2345, 1404

and 1235 cm^{-1}, attributed to surface adsorbed carbonate species, C–O stretching, and C–N stretching vibrations from residual organic intermediates, respectively.

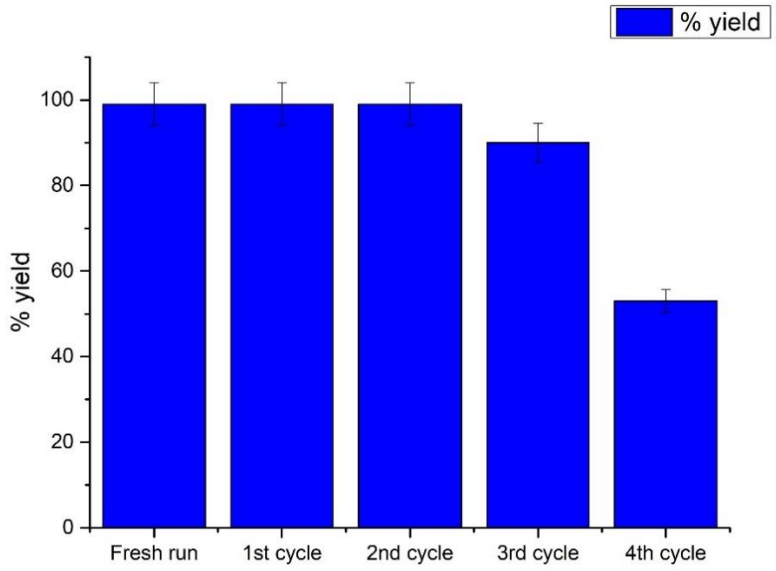

Figure 6. The recyclability of Cu/Pd-N-TiO_2 catalyst for the synthesis of 2-phenylquinoxaline, the activity was maintained for three cycles.

Given the success of the Cu/Pd-N-TiO_2-catalyzed Tandem oxidation procedure, the current scope was explored on the alcohol oxidation-Wittig olefination according to Scheme 1. To our delight, a conversion percentage of 83% was achieved from benzyl alcohol to methyl cinnamate. The potential of Cu/Pd-N-TiO_2 catalyst on the alcohol oxidation-Wittig olefination is currently being evaluated for a wider range of alcohols.

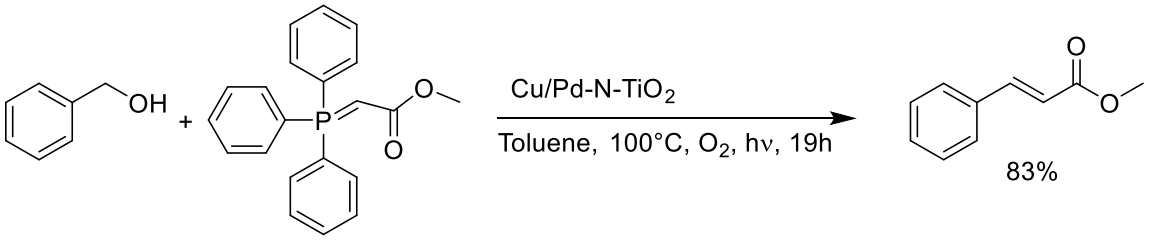

Scheme 1. Olefination of benzyl alcohol through Wittig reaction.

Conclusions

In summary, the Cu/Pd-N-TiO_2 photocatalyst demonstrated remarkable efficiency and recyclability for the synthesis of quinoxaline derivatives in good to excellent yields. Its tolerance toward both electron-donating and electron-withdrawing substituents showcased its versatility across a broad substrate scope. The integration of the oxidation and condensation steps into a single process, and the use of hydroxy carbonyl compounds which are generally more stable and synthetically accessible than 1,2-dicarbonyl analogues, enhanced the practicality of the method. However, the inability to effectively catalyse substrates bearing the

alkyl groups indicated an area for future optimization. Importantly, the protocol utilized visible light as an eco-sustainable energy source and open air as an oxidant. The successful application of the system to the Wittig reaction under visible light demonstrated a promising platform for further exploration in photochemical transformations and sustainable synthesis.

Experimental Section

General. All commercially available reagents, titanium tetraisopropoxide (TTIP), 25% nitric acid, copper nitrate $Cu(NO_3)_2{\cdot}3H_2O$, $Pd(OAc)_2{\cdot}4H_2O$, aqueous ammonia, absolute ethanol and methanol were purchased from Merck, Darmstadt, Germany, and used without further purification. HID Xenon Super Vision HID Head Lamps 35W with broad emission spectrum (400-1000 nm) were used in quinoxaline synthesis.

^1H and ^{13}C NMR spectra were recorded on either a Bruker Avance III 500 or Bruker Avance III 400 spectrometer at frequencies of 500 MHz/400 MHz (^1H) and 125 MHz/100 MHz (^{13}C), respectively. Low and High-Resolution Electrospray Ionization (ESI) Mass Spectra were recorded in a micromass spectrometer using a Time of Flight (TOF) analyzer. Infra-red (IR) spectra were recorded on a Brucker Alpha II FTIR Spectrometer operated by OPUS software. UV/Visible spectra were recorded on a Shimadzu UV/Visible spectrophotometer equipped with Shimadzu ISR- 2600/ISR-2600Plus integrating sphere attachment. Scanning Electron micrographs were collected using a Zeiss Ultra Plus FEG SEM (Germany) the data was processed using SmartSEM imaging software, Oxford X-Max EDX detection system (UK) Aztec EDX analysis software. High-resolution transmission electron micrographs were collected by a JEOL 2100 HRTEM (Japan) GATAN imaging software. Brunauer-Emmett-Teller (BET) surface area, pore volume, and pore size based on nitrogen adsorption-desorption isotherms were analyzed (Anton Paar GmbH, Austria). The phase composition of the prepared catalyst was analyzed by Rigaku p-XRD (Tokyo, Japan) Model – MiniFlex600.

Synthesis of the catalyst

The Cu/Pd-N-TiO_2 catalyst was prepared following the method described by Underwood *et al.*[26] Titanium tetraisopropoxide (TTIP) (10.55 mmol, 3.12 mL) was added dropwise into 15 mL of deionized water, followed by the addition of nitric acid (25%, 4 mL). The solution was left to stir for 30 minutes until it formed a gel. Into this, a solution of copper nitrate $Cu(NO_3)_2{\cdot}3H_2O$ (15 mg) in 2 mL absolute ethanol was added dropwise and stirred for 10 minutes. A solution of palladium acetate $Pd(OAc)_2{\cdot}4H_2O$ (30 mg) in 2 mL absolute ethanol and 1 mL methanol was added dropwise and left to stir for 10 minutes. Ammonia solution was added until a pH of 9 was reached. This was filtered and dried in an oven at 45°C for 1h. The dried sample was ground and then calcined at 350°C for 2h.

General Synthesis for quinoxalines

The reactions were conducted in a solar-simulation 35 W xenon lamps, four lamps were placed in a circular arrangement, with a hot plate in the centre, and a condenser was attached to cooling tubes with a pump for water circulation and an external fan serving as the cooling system. In a quartz tube, 0.1 mmol of hydroxyketone, 0.1 mmol of phenylenediamine, and 30 mg of Cu/Pd-N-TiO_2 catalyst in 3 mL of THF were stirred and irradiated with light at 60 °C for 6 hours. Upon completion, the catalyst was filtered, and the solvent was removed in vacuo. The product was then characterized to provide the following data:

2-Phenylquinoxaline (1a). ^1H NMR (400 MHz, $CDCl_3$) δ: 7.51-7.54 (3H, m), 7.73-7.78 (2H, m), 8.08-8.20 (4H, m), 9.32 (1H, s); ^{13}C NMR (100MHz, $CDCl_3$) δ: 128.0, 128.9, 129.5, 129.6, 130.1, 130.6, 130.7, 130.8, 133.8, 137.3,

141.9, 142.8, 143.8, 152.4 ppm; IR (KBr) cm^{-1} 3055, 2919, 1665, 1605, 1541, 1486, 1443, 1311, 1125; HRMS *m/z*(ESI): ($[M+H]^+$) calculated for $C_{14}H_{11}N_2$ 207.0922, found 207.0918.

6-Bromo-2-phenylquinoxaline / 7-Bromo-2-phenylquinoxaline (1b). ^1H NMR (400 MHz, $CDCl_3$) δ: 7.54-7.60 (3H, m), 7.81-7.88 (1H, m), 7.99-8.05 (1H, m), 8.18-8.21 (2H, d, *J* 7.9 Hz), 8.32-8.36 (1H, dd, *J* 2.3, 17.0 Hz) 9.34 (1H, s) ppm; ^{13}C NMR (100MHz, $CDCl_3$) δ:128.0, 128.7, 129.7, 130.6, 130.8, 131.0, 131.4, 132.4, 143.4, 143.8, 144.4, 152.6 ppm; IR (KBr) cm^{-1} 3047, 1741, 1681, 1595, 1535, 1475, 1445, 1310, 1280; HRMS *m/z*(ESI): ($[M+H]^+$) calculated for $C_{14}H_{10}N_2Br$ 285.0027, found 285.0023.

6,7-Dimethyl-2-phenylquinoxaline (1c). ^1H NMR (400 MHz, $CDCl_3$) δ: 2.55 (6H, s), 7.53-7.60 (3H, m), 7.93 (1H, s), 7.97 (1H, s), 8.19-8.20 (2H,d, *J* 7.9 Hz), 9.26 (1H, s); ^{13}C NMR (100MHz, $CDCl_3$) δ: 20.3, 20.3, 127.4, 128.4, 128.6, 129.1, 129.9, 140.3, 140.9 ppm; IR (KBr) cm^{-1} 3057, 2965, 2915, 2851, 1689, 1624, 1536, 1483, 1447, 1312, 1210; HRMS *m/z*(ESI): ($[M+H]^+$) calculated for $C_{16}H_{15}N_2$ 235.1235, found 235.1230.

2,3-Diphenylquinoxaline (2a). ^1H NMR (400 MHz, $CDCl_3$) δ:7.33-7.35 (6H, m), 7.51-7.53 (4H, dd, *J* 1.6. 8.0 Hz), 7.76-7.78 (2H, dd, *J* 3.5, 6.4 Hz), 8.17-8.19 (2H, m) ppm; ^{13}C NMR (100MHz, $CDCl_3$) δ: 128.7, 129.3, 129.7, 130.3, 130.4, 139.6, 141.7, 153.9 ppm; IR (KBr) cm^{-1} 3054, 1476, 1440, 1343, 1220, 1128; HRMS *m/z*(ESI): ($[M+H]^+$) calculated for $C_{20}H_{15}N_2$ 283.1235, found 283.1239.

6-Bromo-2,3-diphenylquinoxaline (2b). ^1H NMR (400 MHz, $CDCl_3$) δ: 7.33-7.35 (6H, m), 7.50-7.51 (4H, m), 7.83-7.85 (1H, m), 8.02-8.05 (1H, s), 8.36 (1H, s) ppm; ^{13}C NMR (100MHz, $CDCl_3$) δ: 128.7, 128.7, 129.4, 139.5, 130.2, 130.2, 130.9, 131.9, 133.9, 139.0, 140.4, 142.2 ppm; IR (KBr) cm^{-1} 1675, 1592, 1466, 1443, 1337, 1185; HRMS *m/z*(ESI): ($[M+H]^+$) calculated for $C_{20}H_{14}N_2Br$ 361.0340, found 361.0344.

6,7-Dimethyl-2,3-diphenylquinoxaline (2c). ^1H NMR (400 MHz, $CDCl_3$) δ: 2.53 (6H, s), 7.32-7.34 (6H, m), 7.49-7.51 (4H, dd, *J* 2.0, 8.1 Hz), 8.01 (2H, s) ppm; ^{13}C NMR (100MHz, $CDCl_3$) δ: 20.9, 128.4, 128.7, 129.2, 130.4, 139.2, 140.3, 141.5, 152.7 ppm; IR (KBr) cm^{-1} 1691, 1538, 1475, 1339, 1209, 1061, 1018; HRMS *m/z*(ESI): ($[M+H]^+$) calculated for $C_{22}H_{19}N_2$ 311.1548, found 311.1547.

(2,3-Diphenylquinoxaline-6-yl)phenylmethanone (2d). ^1H NMR (400 MHz, $CDCl_3$) δ: 7.34-7.37 (6H, m), 7.51-7.55 (6H, m), 7.64-7.66 (1H, m), 7.89-7.96 (2H, m), 8.0-8.10 (1H, m), 8.21-8.35 (1H, m), 8.56 (1H, s) ppm; ^{13}C NMR (100MHz, $CDCl_3$) δ: 128.4, 128.5, 129.0, 129.2, 129.3, 129.7, 129.8, 129.9, 129.9, 130.1, 132.4, 134.9, 137.2, 138.3, 138.6, 140.2, 143.0, 154.6, 155.2, 195.8 ppm; IR (KBr) cm^{-1} 1654, 1595, 1444, 1396, 1342, 1309, 1262, 1203; HRMS *m/z*(ESI): ($[M+H]^+$) calculated for $C_{27}H_{19}N_2O$ 387.1497, found 387.1500.

2-(4-Chlorophenyl)-3-phenylquinoxaline (3a). ^1H NMR (400 MHz, $CDCl_3$) δ: 7.29-7.36 (2H, d, *J* 8.6 Hz), 7.37-7.39 (3H, m), 7.46-7.48 (2H, d, *J* 8.6 Hz), 7.50-7.52 (2H, m), 7.76-7.79 (2H, m) 8.23 (2H, m) ppm; ^{13}C NMR (100MHz, $CDCl_3$) δ: 128.9, 129.0, 129.6, 129.7, 130.3, 130.7, 130.7, 131.7, 135.7, 137.9, 139.2, 141.6, 141.7, 152.6, 153.7 ppm; IR (KBr) cm^{-1} 3054, 2917, 2850, 1589, 1482, 1339, 1219; HRMS *m/z*(ESI): ($[M+H]^+$) calculated for $C_{20}H_{14}N_2Cl$ 317.0846, found 317.0842.

6-Bromo-2-(4-chlorophenyl)-3-phenylquinoxaline / 7-Bromo-2-(4-chlorophenyl)-3-phenylquinoxaline (3b). ^1H NMR (400 MHz, $CDCl_3$) δ: 7.30-7.32 (2H, d, *J* 8.6 Hz), 7.36-7.39 (3H, m), 7.45-7.51 (4H, m), 7.83-7.86 (1H, dd, *J* 2.2, 8.8 Hz), 8.00-8.04 (1H, m), 8.34 (1H, m) ppm; ^{13}C NMR (100MHz, $CDCl_3$) δ: 124.6, 129.0, 129.8, 130.3, 130.9, 131.7, 131.9, 134.2, 136.0, 137.6, 138.9, 140.4, 142.2 ppm; IR (KBr) cm^{-1} 1666, 1592, 1463, 1337, 1185 ppm; HRMS *m/z*(ESI): ($[M+H]^+$) calculated for $C_{20}H_{13}N_2ClBr$ 394.9951, found 394.9952.

6,7-Dimethyl-2-(4-chlorophenyl)-3-phenylquinoxaline (3c). ^1H NMR (400 MHz, $CDCl_3$) δ: 2.52 (6H, s), 7.28-7.30 (2H, d, *J* 8.5 Hz), 7.34-7.36 (3H, m), 7.43-7.45 (2H, d, *J* 8.5 Hz), 7.47-7.49 (2H, m), 7.90-7.95 (2H, m) ^{13}C NMR (100MHz, $CDCl_3$) δ: 20.9, 128.6, 128.7, 128.8, 128.90, 129.2, 130.2, 131.7, 135.3, 138.3, 139.6, 151.6, 152.7 ppm; IR (KBr) cm^{-1} 2919, 2851, 1458, 1338, 1205, 1085; HRMS *m/z*(ESI): ($[M+H]^+$) calculated for $C_{22}H_{18}N_2Cl$ 345.1159, found 345.1161.

[2-(4-chlorophenyl)-3-phenylquinoxalin-6-yl](phenyl)methanone / [3-(4-chlorophenyl)-2-phenylquinoxalin-6-yl](phenyl)methanone (3d). ^{1}H NMR (400 MHz, $CDCl_3$) δ: 7.30-7.39(5H, m), 7.40-7.41 (6H, m), 7.47-7.51 (1H, m), 7.81-7.90 (2H, m), 8.30 (2H, s), 8.54 (1H, s) ppm; IR (KBr) cm^{-1} 2920, 2852, 1654, 1592, 1448, 1398, 1310, 1263.

2,3-Bis(4-methoxyphenyl)quinoxaline (4a). ^{1}H NMR (400 MHz, $CDCl_3$) δ: 3.81 (6H, s), 6.84-6.86 (4H, d, *J* 9.2 Hz), 7.46-7.48 (4H, d, *J* 8.8 Hz), 7.68-7.71 (2H, dd, *J* 3.5, 6.4 Hz), 8.09-8.11 (2H, dd, *J* 3.4, 6.4 Hz) ppm; ^{13}C NMR (100MHz, $CDCl_3$) δ: 55.8, 114.3, 129.4, 130.0, 131.7, 132.2, 141.5, 153.5, 160.7 ppm; IR (KBr) cm^{-1} 1603, 1508, 1456, 1392, 1343, 1288, 1239, 1170; HRMS *m/z*(ESI): ([M+H]$^{+}$) calculated for $C_{22}H_{19}N_2O_2$ 343.1447, found 343.1445.

6-Bromo-2,3-bis(4-methoxyphenyl)quinaxoline (4b). ^{1}H NMR (400 MHz, $CDCl_3$) δ: 3.84 (6H, s), 6.88-6.90 (4H,d, 8.61 Hz), 7.50-7.53 (4H, dd, *J* 3.3, 8.7 Hz), 7.83-7.85 (1H, dd, *J* 2.2, 8.7 Hz), 8.15-8.17 (1H, d, 9.1 Hz), 8.44 (1H, s) ppm; IR (KBr) cm^{-1} 1654, 1599, 1507, 1408, 1336, 1245, 1170, 1021; HRMS *m/z*(ESI): ([M+H]$^{+}$) calculated for $C_{22}H_{18}N_2O_2Br$ 421.0552, found 421.0554.

2,3-Bis(4-methoxyphenyl)-6,7-dimethylquinaxoline (4c). ^{1}H NMR (400 MHz, $CDCl_3$) δ: 2.50 (6H, s), 3.82 (6H, s), 6.85-6.87 (4H, d, *J* 8.8 Hz), 7.45-7.47 (4H, d, *J* 8.6 Hz), 7.87 (2H, s) ppm; IR (KBr) cm^{-1} 2920, 2851, 1654, 1601, 1510, 1454, 1245, 1173; HRMS *m/z*(ESI): ([M+H]$^{+}$) calculated for $C_{24}H_{23}N_2O_2$ 371.1760, found 371.1763.

Acknowledgements

The authors would like to acknowledge the funding for this project through the Eskom TESP and UTT programmes, as well as support from the University of KwaZulu-Natal.

Supplementary Material

For spectra of synthesized compounds, please see the Supplementary Information file.

References

1. Chen, J.; Cen, J.; Xu, X.; Li, X. *Catal. Sci. Technol.* **2016**, *6*, 349-362. https://doi.org/10.1039/c5cy01289a
2. Bagheri, S.; Muhd Julkapli, N.; Bee Abd Hamid, S. *Sci. World J.* **2014**, *2014*, 727496. https://doi.org/10.1155/2014/727496
3. Friedmann, D.; Hakki, A.; Kim, H.; Choi, W.; Bahnemann, D. *Green Chem.* **2016**, *18*, 5391-5411. https://doi.org/10.1039/c6gc01582d
4. Al-Hajji, L. A.; Ismail, A. A.; Bumajdad, A.; Alsaidi, M.; Ahmed, S. A.; Al-Hazza, A.; Ahmed, N. *Environ. Technol. Innovation* **2021**, *24*, 101958. https://doi.org/10.1016/j.eti.2021.101958
5. Kumar, A.; Khan, M.; He, J.; Lo, I. M. C. *Water Res.* **2020**, *170*, 115356. https://doi.org/10.1016/j.watres.2019.115356

6. Zhang, Q.; Quan, X.; Wang, H.; Chen, S.; Su, Y.; Li, Z. *Sci. Rep.* **2017**, *7*, 3128. https://doi.org/10.1038/s41598-017-03347-y
7. Kuo, C.-Y.; Jheng, H.-K.; Syu, S.-E. *Environ. Technol.* **2021**, *42*, 1603-1611. https://doi.org/10.1080/09593330.2019.1674930
8. Skolia, E.; Gkizis, P. L.; Kokotos, C. G. *ChemPlusChem* **2022**, *87*, e202200008. https://doi.org/10.1002/cplu.202200008
9. Liu, Y.; Jiang, X.; Chen, L.; Cui, Y.; Li, Q.-Y.; Zhao, X.; Han, X.; Zheng, Y.-C.; Wang, X.-J. *J. Mater. Chem. A* **2023**, *11*, 1208-1215. https://doi.org/10.1039/D2TA07177K
10. Huang, C.; Wen, Y.; Ma, J.; Dong, D.; Shen, Y.; Liu, S.; Ma, H.; Zhang, Y. *Nat. Commun.* **2021**, *12*, 320. https://doi.org/10.1038/s41467-020-20521-5
11. Heidari, A.; Safa, K. D.; Teimuri-Mofrad, R. *Mol. Catal.* **2023**, *547*, 113338. https://doi.org/10.1016/j.mcat.2023.113338
12. Lang, X.; Chen, X.; Zhao, J. *Chem. Soc. Rev.* **2014**; *43*, 473-486. https://doi.org/10.1039/C3CS60188A
13. Wu, J.; Kozlowski, M. C. *Org. Lett.* **2023**, *25*, 907-911. https://doi.org/10.1021/acs.orglett.2c04122
14. Tariq, S.; Somakala, K.; Amir, M. *Eur. J. Med. Chem.* **2018**, *143*, 542-557. https://doi.org/10.1016/j.ejmech.2017.11.064
15. Patinote, C.; Deleuze-Masquefa, C.; Kaddour, K. H.; Vincent, L. A.; Larive, R.; Zghaib, Z.; Guichou, J. F.; Assaf, M. D.; Cuq, P.; Bonnet, P. A. *Eur. J. Med. Chem.* **2021**, *212*, 113031. https://doi.org/10.1016/j.ejmech.2020.113031
16. Hu, W.; Gao, S.; Zhao, L. X.; Guo, K. L.; Wang, J. Y.; Gao, Y. C.; Shao, X. X.; Fu, Y.; Ye, F. *Pest Manag. Sci.* **2022**, *78*, 938-946. https://doi.org/10.1002/ps.6703
17. Alanazi, M. M.; Elkady, H.; Alsaif, N. A.; Obaidullah, A. J.; Alanazi, W. A.; Al-Hossaini, A. M.; Alharbi, M. A.; Eissa, I. H.; Dahab, M. A. *J. Mol. Struct.* **2022**, *1253*, 132220. https://doi.org/10.1016/j.molstruc.2021.132220
18. Fayed, E. A.; Ebrahim, M. A.; Fathy, U.; Saeed, H. S. E.; Khalaf, W. S. *J. Mol. Struct.* **2022**, *1267*, 133578. https://doi.org/10.1016/j.molstruc.2022.133578
19. Abdelgalil, M. M.; Ammar, Y. A.; Elhag Ali, G. A. M.; Ali, A. K.; Ragab, A. *J. Mol. Struct.* **2023**, *1274*, 134443. https://doi.org/10.1016/j.molstruc.2022.134443
20. Yzeiri, X.; Sangiorgi, N.; Gambassi, F.; Barbieri, A.; Calamante, M.; Franchi, D.; Coppola, C.; Sinicropi, A.; Ventura, B.; Mordini, A.; et al. *Dyes Pigm.* **2025**, *232*, 112455. https://doi.org/10.1016/j.dyepig.2024.112455
21. Abid, Z.; Ali, L.; Gulzar, S.; Wahad, F.; Ashraf, R. S.; Nielsen, C. B. *Beilstein J. Org. Chem.* **2023**, *19*, 1694-1712. https://doi.org/10.3762/bjoc.19.124
22. Alsaif, N. A.; Dahab, M. A.; Alanazi, M. M.; Obaidullah, A. J.; Al-Mehizia, A. A.; Alanazi, M. M.; Aldawas, S.; Mahdy, H. A.; Elkady, H. *Bioorg. Chem.* **2021**, *110*, 104807. https://doi.org/10.1016/j.bioorg.2021.104807
23. Kumar, A.; Dhameliya, T. M.; Sharma, K.; Patel, K. A.; Hirani, R. V.; Bhatt, A. J. *J. Mol. Struct.* **2022**, *1259*, 132732.

https://doi.org/10.1016/j.molstruc.2022.132732
24. Taylor, R.; Robinson, R. *Synlett* **2005**, *2005*, 1003-1005. https://doi.org/10.1055/s-2005-864830
25. Chan Sik Cho, S. G. O. *J. Mol. Catal. A: Chem.* **2007**, *276*, 205-210. https://doi.org/10.1016/j.molcata.2007.07.014
26. Underwood, T. M.; Robinson, R. S. *New J. Chem.* **2020**, *44*, 19201-19211. https://doi.org/10.1039/c9nj05034e
27. File, P. D. *Joint Committee on Powder Diffraction Standards, ASTM, Philadelphia, PA*; Card 21-1272–PDF. Search in, 1969.
28. Zedan, A. F.; Gaber, S.; AlJaber, A. S.; Polychronopoulou, K. *Nanomaterials* **2021**, *11*, 1675. https://doi.org/10.3390/nano11071675
29. Alshammari, H. M. *Processes* **2021**, *9*, 1590. https://doi.org/10.3390/pr9091590
30. Khalfaoui, M.; Knani, S.; Hachicha, M. A.; Lamine, A. B. *J. Colloid. Interface Sci.* **2003**, *263*, 350-356. https://doi.org/10.1016/s0021-9797(03)00139-5
31. Serpone, N. *J. Phys. Chem.* **2006**, *110*, 24287-24293. https://doi.org/10.1021/jp065659r
32. Lisowski, P.; Colmenares, J. C.; Łomot, D.; Chernyayeva, O.; Lisovytskiy, D. *J. Mol. Catal. A: Chem.* **2016**, *411*, 247-256. https://doi.org/10.1016/j.molcata.2015.10.031
33. Azami, M. S.; Nawawi, W. I.; Jawad, A. H.; Ishak, M. A. M.; Ismail, K. *Sains Malaysiana* **2017**, *46*, 1309-1316. https://doi.org/10.17576/jsm-2017-4608-17
34. Bryden, M. A.; Millward, F.; Lee, O. S.; Cork, L.; Gather, M. C.; Steffen, A.; Zysman-Colman, E. *Chem. Sci.* **2024**, *15*, 3741-3757. https://doi.org/10.1039/d3sc06499a
35. Qiao, J.; Song, Z. Q.; Huang, C.; Ci, R. N.; Liu, Z.; Chen, B.; Tung, C. H.; Wu, L. Z. *Angew. Chem. Int. Ed. Engl.* **2021**, *60*, 27201-27205. https://doi.org/10.1002/anie.202109849
36. Zhang, T.; Chen, Y.; Yang, X.; Chen, J.; Zhong, J.; Li, J.; Li, M.; Wan, Z. *Mater. Today Chem.* **2023**, *28*, 101358. https://doi.org/10.1016/j.mtchem.2022.101358
37. Bartholomew, C. H. *App. Catal. A: Gen.* **2001**, *212*, 17-60. https://doi.org/10.1016/S0926-860X(00)00843-7
38. Kunene, A.; Leteba, G.; van Steen, E. *Catal. Lett.* **2021**, *152*, 1760-1768. https://doi.org/10.1007/s10562-021-03760-z